ACS Catalysis

pubs.acs.org/acscatalysis Research Article

Mechanistic Insights into the Formation of CO and C_2 Products in Electrochemical CO_2 Reduction—The Role of Sequential Charge Transfer and Chemical Reactions

Rileigh Casebolt DiDomenico, Kelsey Levine, Laila Reimanis, Héctor D. Abruña, and Tobias Hanrath*

Cite This: ACS Catal. 2023, 13, 4938–4948 Read Online

ACCESS | Metrics & More | Article Recommendations | Supporting Information

ABSTRACT: The electrochemical reduction of CO_2 presents an attractive opportunity to not only valorize CO_2 as a feedstock for chemical products but also to provide a means to effectively store renewable electricity in the form of chemical bonds. The recent surge of experimental and computational studies of electrochemical CO_2 reduction (ECR) has brought about significant scientific and technological advances. Yet, considerable gaps in our understanding of and control over the reaction mechanism persist, in particular for the formation of products. Moreover, while theoretical and computational studies have proposed many candidate reaction pathways, comprehensively reconciling these models with experimental observations remains challenging and elusive. The conventional electrochemical analysis of catalyst activity and selectivity generally relies on steady-state measurements. In a departure from this convention, we show in this study that time-resolved measurements (i.e., chronoamperometry) provide a powerful diagnostic tool to gain valuable insights into the complex interplay of electrochemical reactions, chemical reactions, and mass transport. We show that the initial stages of the ECR reaction show signatures of an electrochemical reaction followed by a homogeneous chemical reaction. These signatures have important mechanistic implications and inform dominant reaction pathways, specifically for the sequential electron and proton transfer steps leading to the formation of formate intermediates (*$COOH^-$). We hope that the methods and insights presented in this work will inspire future studies to exploit chronoamperometric analysis to resolve outstanding questions in ECR and other multi-step electrochemical reaction pathways.

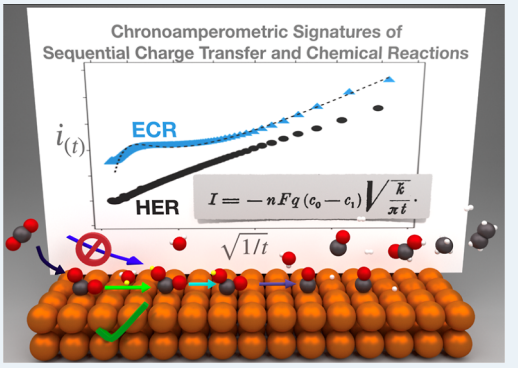

KEYWORDS: *electrochemical CO_2 reduction, chronoamperometry, reaction pathways, sequential electron and proton transfer, Cottrell analysis*

INTRODUCTION

Translate your challenges into opportunities; this maxim applies equally well at the personal level as at the global level. The now evident impacts of climate change underscore the urgent need to address the challenge of reducing anthropogenic CO_2 emissions by transitioning toward a more sustainable energy landscape. Whereas recent years have witnessed remarkable advances in the deployment of solar and wind energy, the system-level integration of these inherently intermittent energy sources has introduced additional challenges of storing the energy across various timescales. Storing energy in the form of chemical bonds, as nature does, is an attractive solution, and electrochemical processes offer a compelling opportunity to translate CO_2 from an environmental liability into a feedstock for chemical products and fuels.

Thanks to intensive recent research activities, the science and engineering of electrochemical CO_2 reduction (ECR) have progressed on several fronts, including experimental and computational advances in understanding the mechanism,[1−4] catalyst development,[5−8] and advances in reactor design such as gas diffusion electrode flow cells and membrane electrode assemblies to achieve industrially relevant current densities.[9−12] Beyond improving the conversion efficiency (i.e., electrocatalytic activity), directing the reduction of CO_2 toward the formation of specific value-added products defines a key goal to bring this process to fruition.[13,14] Copper, by virtue of its unique ability to stabilize reaction intermediates like *CO and *H, enables the formation of higher-order carbon products.[15] C_2 products, like ethylene and ethanol, are particularly desirable because they can be used as feedstocks in established chemical industries and have a market size larger than 80 million tons per year and a higher market price per ton than C_1 products.[16]

Received: December 7, 2022
Revised: February 19, 2023
Published: March 27, 2023

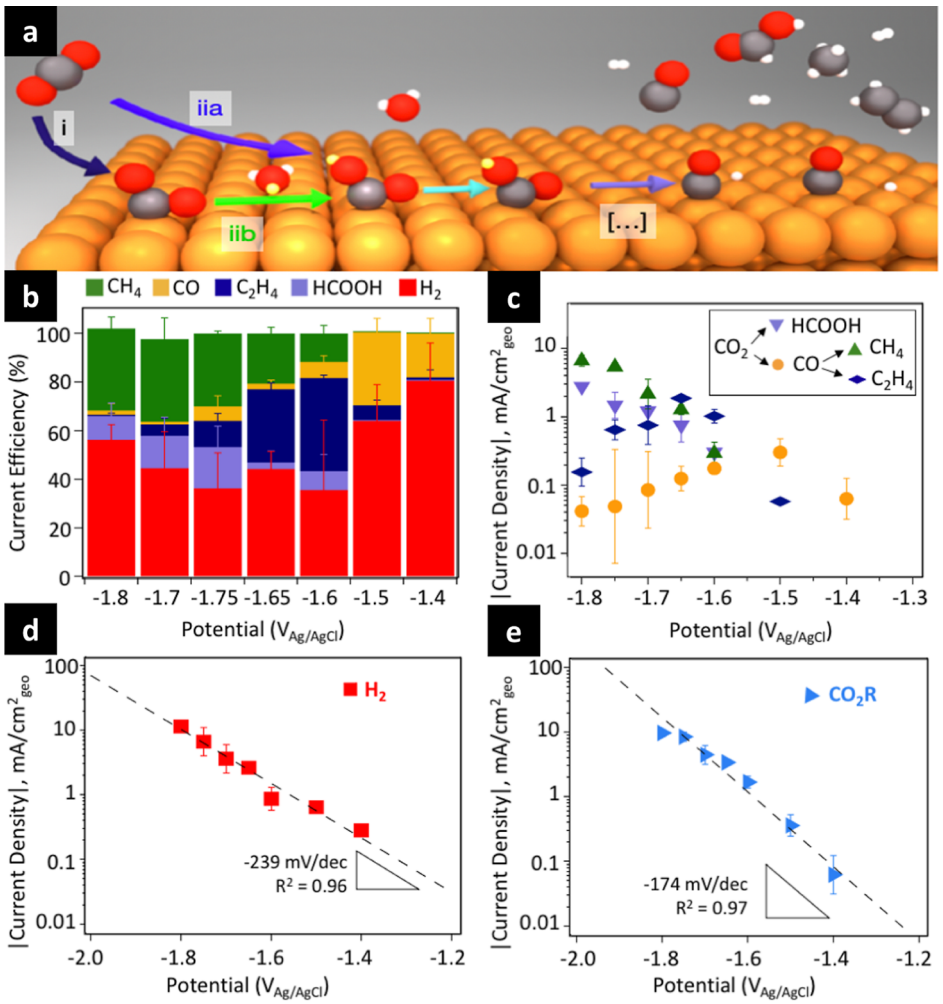

Figure 1. (a) Schematic illustration showing the possible transformation of CO_2 to $*COOH^-$ via a concerted proton electron transfer (path iia, purple arrow) or sequential electron transfer to form $*CO_2^-$ (path i, blue arrow), followed by a proton transfer to form *COOH (path iib, green arrow) and another electron transfer to form $*COOH^-$ (light blue arrow). Gray = carbon, red = oxygen, white = hydrogen, and transferred proton = yellow. (b) Selectivity of ECR at different potentials plotting average ± one standard deviation from $n = 3$ separate replicates. (c) Tafel plot comparing the activities of CO (yellow circles), CH_4 (green triangles), C_2H_4 (blue diamonds), and HCOOH (purple upside-down triangles). Inset: figure legend and general schematic of CO_2 to major ECR products. (d) Tafel plot of HER activity. (e) Tafel plot of total ECR activity.

Research endeavors to steer the reaction toward better C_2 selectivity have provided new insights into the role of modifying the electrolyte and/or microenvironment,[17−20] catalyst faceting,[21,22] roughening the surface,[23,24] introducing mixed-valence copper species,[25−28] nanostructuring the catalyst to introduce defects or to confine intermediates,[29−31] and pulsing the applied voltage.[32−36] Future endeavors to bring these advances to fruition stand to benefit from answers to outstanding questions about the fundamental mechanisms within the complex reaction network. Computational studies, particularly density functional theory (DFT) calculations of binding and activation energies, continue to provide detailed information into the energetics and possible reaction pathways. Yet, interpreting experimental observations in the context of these computational predictions remains challenging.[37]

Transient processes (i.e., non-steady-state) introduce not only additional complications but also opportunities to better understand the dynamic interplay of electron transfer, competing chemical reactions, and mass transport. Time-resolved operando spectroscopy (e.g., Raman and IR)[38−40] studies have provided important insights into these processes. However, whereas electrochemical measurements of the ECR are commonly done under steady-state conditions, the experiments and analysis described in this paper show that simple transient measurements provide important new insights into the competing sub-processes and the reaction mechanism. Specifically, we show that analysis of the transient current in response to a step change in voltage (i.e., chronoamperometry analyzed by the Cottrell model) reveals that the ECR involves electrochemical reactions at the electrode surface followed by homogeneous chemical reactions in the proximate electrolyte environment. Our results are consequential to enable future advances in the field, as this analysis helps provide the necessary experimental mechanistic insights to identify the operative reaction pathways. We anticipate that these insights will help enable future advances toward efficient and scalable CO_2 to C_2 transformation pathways.

RESULTS AND DISCUSSION

Critical steps in the electrochemical reduction of CO_2 on the surface of a copper electrode are illustrated in Figure 1a. We note that the detailed mechanistic pathways are sensitive to the electrode structure, the pH, and spectator ions in the electrical

https://doi.org/10.1021/acscatal.2c06043
ACS Catal. 2023, 13, 4938−4948

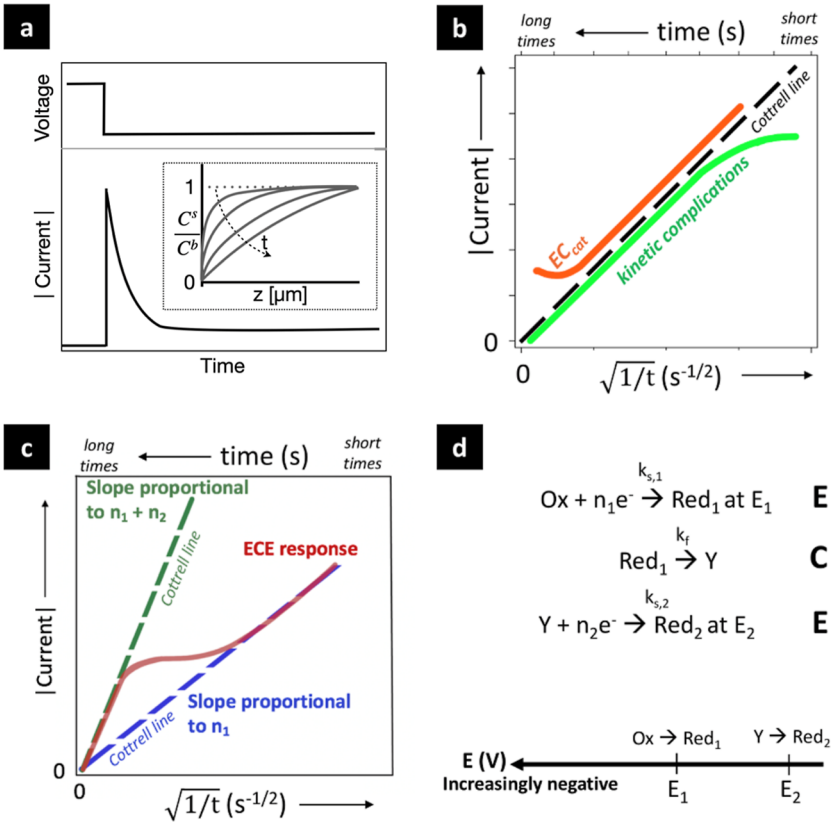

Figure 2. (a) Example current versus time response following a potential step for an electrochemically reversible system where the current is a function of $\sqrt{1/t}$. The inset illustrates the spatiotemporal evolution of the reactant concentration profile following the step change. (b) Schematic illustration of a Cottrell plot for a reversible system (black dashed Cottrell line), a system with kinetic complications (green line), and an EC_{cat} system (orange line). (c) Schematic illustration of a Cottrell plot for an ECE system (red line), where at short times, the current is proportional to the number of electrons in the first electrochemical step (blue dashed line), and at long times, the current is proportional to the cumulative number of electrons in the first and second electrochemical steps (green dashed line). (d) ECE mechanism in which species Ox gets reduced to Red_1 at a potential of E_1 with an electron transfer rate constant of $k_{s,1}$. Then, Red_1 is chemically reacted to form Y with a rate constant of k_f (assuming $k_b = 0$). Then, Y is reduced to Red_2 at a potential of E_2 with an electron transfer rate constant of $k_{s,2}$. Potential number line shows the relative position of the first electrochemical reaction to the second electrochemical reaction.

double layer.[14] We focus here on a simplified depiction of these processes on an idealized Cu(100) surface. The first step involves either the formation of surface-adsorbed $*CO_2^-$ or *COOH intermediates.[14,41] The adsorbed intermediates can then go on to form formate, which cannot be further reduced,[42] or to CO and then on to other reduction products.[4] Whether the hydrogenation to form *COOH− proceeds via a concerted (i.e., proton-coupled electron transport: PCET, pathway iia) or a sequential electron and proton transfer (pathways i and iib, respectively, in Figure 1a) is currently not well understood. This defines one of the mechanistic questions at the focus of our study. Below, we will first establish basic ECR trends under potentiostatic conditions and then turn to chronoamperometric methods to address the mechanistic question above in the context of pathways defined by either sequential versus concerted electrochemical and homogeneous chemical reactions (Figure 1a).

The ability to stabilize both *COOH and *CO intermediates is the defining characteristic of copper as the only pure metal electrode that can reduce CO_2 beyond two electrons with appreciable efficiency.[15] CO is known as a critical intermediate in the formation of other hydrocarbons.[43] However, efforts to establish a detailed and comprehensive reaction mechanism for reduction products beyond CO are complicated by the diversity of reaction products. Previous work by Kuhl et al. identified 16 products in 0.1 M $KHCO_3$ over a range of potentials.[13] Our experiments (in 1 M KCl electrolyte) identify five major products (H_2, CO, HCOOH, CH_4, and C_2H_4), as illustrated on the right side of Figure 1b.

The distribution of products (i.e., Faradaic efficiency) depends on the applied reduction potential, as shown in Figure 1b. Details of the experimental configuration for the electrochemical measurements are provided in the Methods section below. All electrochemical potentials discussed below are referenced to a Ag/AgCl electrode. The corresponding partial current densities shown in Figure 1c illustrate several common trends. With increasingly negative reduction potentials, the first CO_2 reduction product at −1.4 V is CO, which is formed alongside H_2 from the hydrogen evolution reaction (HER) at an approximately fourfold higher rate. Pushing the system toward higher overpotentials (more negative reduction potentials) leads to the formation of C_2H_4 (starting at −1.5 V and increasing to about 38% FE at −1.6 V). At reduction potentials beyond −1.5 V, two key trends are notable. First, the shift toward C_2H_4 coincides with the diminished formation of CO, which is consumed to make C_2 products.[14,43,44] Second, for reduction potentials from −1.6 to −1.8 V, the formation of CH_4 appears to outcompete C_2H_4. This order of activity from CO to C_2H_4 to CH_4 at increasingly negative potentials is generally valid for a range of electro-

https://doi.org/10.1021/acscatal.2c06043
ACS Catal. 2023, 13, 4938−4948

lytes,[45] although the exact onset potential will be system-specific due to variations in the potential of zero charge (E_{pzc}) with electrolyte composition and concentration.[43,46] Possible reaction pathways leading to the formation of C_1 and C_2 products have been discussed in the literature.[14,47]

The interfacial charge transfer kinetics underlying the relationships between the measured current, i, and the applied overpotential, η, described above are governed by the Butler–Volmer equation

$$i = i_0[e^{-\alpha(\frac{nF}{RT})\eta} - e^{(1-\alpha)(\frac{nF}{RT})\eta}] \quad (1)$$

which describes the net current between the reduction and oxidation processes multiplied by the exchange current, i_0.[48] In eq 1, F, R, T, n, and α are Faraday's constant, the ideal gas constant, the temperature, the number of electrons transferred, and the transfer coefficient, respectively. Practical electrolysis currents require high overpotentials. In this regime, the exponential relationship between current and overpotential can be described by the Tafel equation[48]

$$\eta = a + b \log i \quad (2)$$

where $a = 2.3RT/\alpha F \log i_0$ and $b = -2.3RT/\alpha F$. Analysis of the experimental current–voltage relation in terms of overpotential and Tafel slope provides critical insights into the kinetics of competing reactions. For an electrochemically reversible (meaning fast kinetics) one-electron transfer process at room temperature, the theoretical Tafel slope, a, should be 118 mV/dec.[48] The experimentally observed Tafel slopes for ECR and HER processes are 174 and 239 mV/dec, respectively (Figure 1d,e). Moreover, the side-by-side comparison of the ECR and HER Tafel slopes reveals that the latter is relatively slow on copper compared to the former on the time scale of our experiment. This trend is consistent with thermodynamic arguments based on theoretical binding energy scaling relations, which show that Cu has a negative CO adsorption energy while having a positive H binding energy.[15] Individually measured Tafel slopes for CO, C_2H_4, HCOOH, and CH_4 are 148, 94, 216, and 141 mV/dec, respectively (see Section S2). These values do not fall neatly on cardinal values (40, 60, and 120 mV/dec), which is common in the ECR literature and implies the existence of physical nonidealities, which obscure the deduction of mechanistic information from Tafel slope data alone.[49] However, whereas the seemingly sluggish, non-ideal ECR kinetics present a practical challenge, they also present a scientific opportunity to probe transient behavior using chronoamperometric analysis, as shown below.

We now turn to time-resolved electrochemical measurements. Beyond insights into the thermodynamic and kinetic aspects of the underlying reactions, a comprehensive description of the heterogeneous electrocatalysis also needs to consider competing dynamic subprocesses, including mass transport and other coupled chemical reactions.[48] Time-resolved electrochemical measurements not only provide an opportunity to disentangle these effects but also offer new mechanistic insights into microkinetic steps. Chronoamperometric analysis, in particular, focuses on the transient electrochemical current in response to a step change of the applied potential. As schematically illustrated in the inset of Figure 2a, stepping the electrode toward a negative potential will initiate CO_2 reduction and create a concentration gradient between the surface concentration $C^s_{CO_2}$ and bulk concentration $C^b_{CO_2}$ outside of the boundary layer. The diffusive mass transport of CO_2 to replenish material consumed at the electrode can be modeled by Fick's laws. Under these conditions, the current is proportional to the concentration gradient over the boundary layer; hence, the maximum current is achieved when $C^s_{CO_2} = 0$. Cottrell showed that the diffusion-controlled transient current can be described as[48]

$$i_{(t)} = nFAC^b_{CO_2}\left(\frac{D}{\pi t}\right)^{1/2} \quad (3)$$

where A and D refer to the electrode area and species diffusivity, respectively.

An important consequence of the Cottrell equation is that the transient current in a diffusion-limited system should scale as $t^{-1/2}$. A deviation from this so-called Cottrell line suggests that the electrochemical reaction is impacted by other processes, such as kinetic limitations or chemical changes.[50] We hypothesized that these chronoamperometric signatures could provide essential clues on outstanding mechanistic questions. Specifically, if electron and proton transfer shown in Figure 1a is a sequential process, then the Cottrell analysis should reveal a characteristic fingerprint signature of decoupled (i.e., sequential) electrochemical and homogeneous chemical reactions. Before applying the Cottrell analysis to the ECR, we will summarize three general characteristic examples of the diagnostic power of the Cottrell formalism with regards to reaction mechanisms (Figure 2b,c). (Additional information and explanations of the Cottrell method are provided in the Section S10.)

First, in the case of an electrochemically irreversible (slow kinetics) system or a system with some pre-kinetics (i.e., a chemical reaction preceding the electrochemical step, denoted as CE), the transient current response will be characterized by negative deviations from the Cottrell line at short times (Figure 2b, green line). Slow reaction kinetics can lead to a non-zero surface concentration, which reduces the initial diffusion-limited current below the Cottrell line.[50] A second type of deviation from the Cottrell line can arise in an EC_{cat} system involving an electrochemical step followed by a chemical step, regenerating more of the original reactant. In this case, the transient current response will be above the Cottrell line at long times as there is more reactant present than what would be predicted by the mass transport-limited current (Figure 2b, orange line).[50] Short-time versus long-time scales are relative, where short time indicates the initial time after a potential step and long time indicates some time after that.

The sequence of an electrochemical reaction followed by a chemical reaction can be extended to include additional subsequent reactions. One possible scenario is a third electrochemical reaction at the electrode surface (i.e., EC-E for simplicity, written as ECE here). Alternatively, the product of the first two steps can react in a disproportionation reaction (i.e., EC-DISP). We focus our analysis here on the first version (ECE) and provide additional discussion of the EC-DISP mechanism in the Supporting Information (Section S10). Consider the case of an ECE mechanism wherein the first electrochemical step occurs at a potential more negative than that of the second (i.e., the first electrochemical reaction requires a higher driving force than the second). The transient response of this scenario is characterized by two distinct Cottrell regions (Figure 2c): (i) at short times, the system is described by a first Cottrell line corresponding to the current

https://doi.org/10.1021/acscatal.2c06043
ACS Catal. 2023, 13, 4938–4948

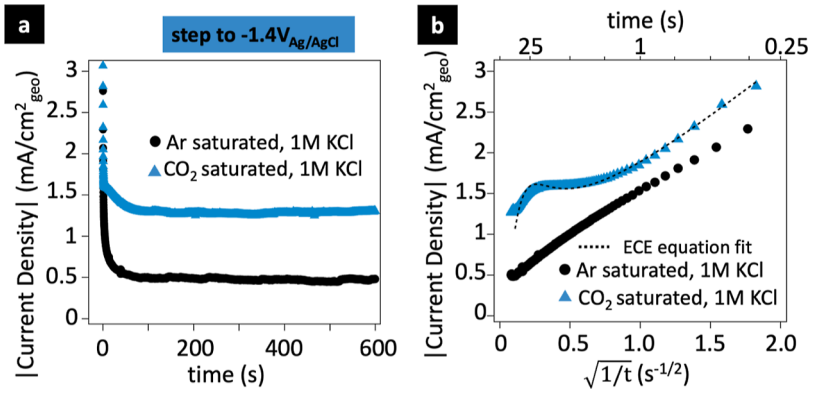

Figure 3. (a) Current density versus time when stepping from −0.6 to −1.4 V for 10 min in CO_2-saturated (blue triangles) and Ar-saturated (black circles) 1 M KCl. (b) Corresponding Cottrell plot (I vs $t^{-1/2}$) for step to −1.4 V in CO_2-saturated (blue triangles) and Ar-saturated (black circles) 1 M KCl with ECE fit (black dotted line) to eq 4, R^2 = 0.99.

flow in the first electrochemical step and (ii) a second Cottrell line at long times corresponding to the cumulative current flow associated with both the first and second electrochemical steps.[50] In the context of the sequential reactions, the transient current can be explained as follows: At potentials less negative than the formal reducing potential for the first electrochemical step, there is no observable current. Even though the second electrochemical step can thermodynamically occur at a less negative potential, the reaction does not occur since the necessary reactants for the second electrochemical step have yet to be formed. Pushing the potential more negative than the formal reduction potential for the first electrochemical step generates an electrochemical current due to the conversion of Ox to Red_1 (Figure 2d, first E step). At short times, the overall system current is proportional to that first electrochemical step. However, with extended reaction time and ongoing transformation of Red_1 to Y (Figure 2d, chemical reaction C step), the second electrochemical step, Y to Red_2, can now occur (Figure 2d, second E step). Consequently, at long times, the observed current is larger than the current from the first electrochemical reaction alone and instead scales in proportion to the sum of the two electrochemical steps.[50]

Assuming that the initial concentrations of Red_1 and Y are zero (since initially only CO_2 is present) and neglecting the reverse reaction of Y → Red_1 (on the basis that the Tafel analysis in Figure 1d and individual Tafel slopes are indicative of an irreversible reaction), although the interpretation of the Tafel slopes involves some nuances, as discussed above,[49] we can describe the transient current associated with an ECE mechanism as[50]

$$i = \left(\frac{a}{t}\right)^{1/2}(n_1 + n_2(1 - e^{-k_f t})),$$
$$\text{where } a = FC^{b}_{Ox}\left(\frac{D}{\pi}\right)^{1/2} \quad (4)$$

In this equation, i is the measured current, t is the time, n_1 and n_2 are the number of electrons transferred in the first and second electrochemical steps, respectively, k_f is the forward reaction rate constant for the chemical step, F is Faraday's constant, D is the diffusion coefficient, and C^{b}_{ox} is the bulk concentration of the oxidized species. Since the HER and ECR reactions are happening simultaneously, the parameters in this equation result from the combined contribution of both reactions to the measured current, which will be discussed in more detail below.

We now apply the chronoamperometric analysis of ECR and the HER at the heart of this study. We will first examine the system response to a step change to −1.4 V, for which only CO and H_2 are formed, and then, we will apply the same analysis to the more complex combination of reaction products formed in a step change to −1.6 V. Our experiments were performed in KCl electrolyte as this affords better control over the product distribution toward CO and C_2 products[45] and because unbuffered electrolytes are not an uncommon electrolyte choice for CO_2 reduction experiments.[51,52] We provide additional experiments and discussion in the Supporting Information (Sections S12 and S13) to confirm that although KCl electrolyte provides an unbuffered environment, pH changes during the experiment do not impact the Cottrell analysis described below.

To delineate between ECR and the HER, we performed a control experiment in Ar-saturated (i.e., CO_2-free) KCl electrolyte. The transient current (black trace in Figure 3b) shows that the HER closely follows the Cottrell line (current decays as $t^{-1/2}$), indicative of a diffusion-limited system. To account for possible pH differences between CO_2-saturated KCl (pH = 3.8) and Ar-saturated KCl (pH = 7), we also conducted an Ar-saturated control experiment in a 1 M KCl + 0.0016 M HCl solution (pH = 3.8), which confirmed that in the absence of CO_2, the transient current of the HER decays linearly with $t^{-1/2}$ (Section S12). In pronounced contrast to the transient response of the HER, the same experiment and analysis of a CO_2-saturated electrolyte reveal a notably different response with a clear deviation from the Cottrell line.

The specific nonlinear response of the ECR shown in Figure 3b is indicative of a reaction pathway involving electrochemical and chemical reactions in sequence. This transient signature is consistent with an ECE process in which the second electrochemical step proceeds at a less negative potential than the first.[50,53] We provide additional analysis and discussion in the Supporting Information to validate this interpretation against other noise factors, including the confirmation of isothermal conditions (Section S7), the negligible impact of specific adsorption (Section S3), and the possible role of competing EC-E and EC-DISP reaction pathways (Section S10). We also note that the mechanistic interpretation of the deviation from the Cottrell response as a clear signature of sequential charge transfer and chemical

https://doi.org/10.1021/acscatal.2c06043
ACS Catal. 2023, 13, 4938−4948

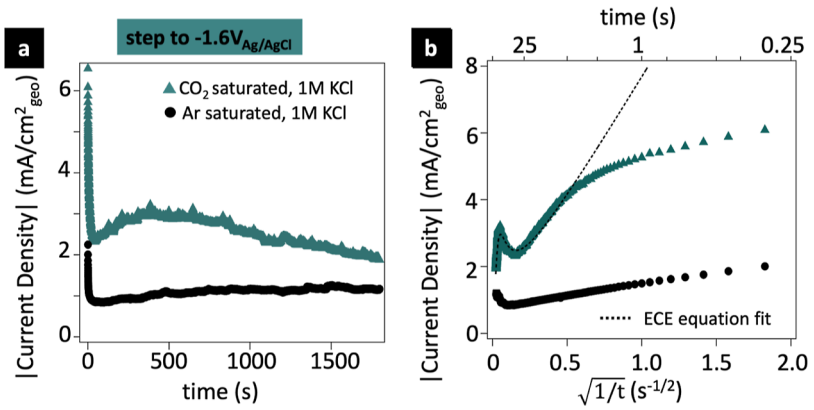

Figure 4. (a) Current density versus time when stepping from −0.6 to −1.6 V for 30 min in CO_2-saturated (filled turquoise triangles) and Ar-saturated (black circles) 1 M KCl. (b) Corresponding Cottrell plot (I vs $t^{-1/2}$) for step to −1.6 V in CO_2-saturated (filled turquoise triangles) and Ar-saturated (black circles) 1 M KCl with ECE fit (black dotted line) to eq 4. R^2 = 0.96 when fit from $0 < t^{-1/2} < 0.6$. At $t^{-1/2} > 0.6$, data bends off the Cottrell line due to kinetic complications.

reactions is robust against changes in the local pH during the experiment (Sections S12 and S13).

Quantitative analysis of the slopes of the two Cottrell lines provides insights into the mechanism of the sequence of reactions based on an electrochemical transfer of n_1 electrons followed by a homogeneous chemical step (within the electrolyte) and another electrochemical transfer of n_2 electrons.[48] We used a nonlinear least squares method, which iterates through possible parameter ($0 < a$, n_1, n_2, and $k_f < \infty$) estimates, to find the best fit for the data to eq 4. This fit does not assume any species-specific values, and since both the HER and ECR contribute to the measured current, the calculated fit parameters (n_1, n_2, C^b_{ox}, and D) in eq 4 are impacted by both processes. Since the HER has a linear Cottrell response (Figure 3b), indicative of a diffusion-limited electrochemical step with no separate chemical step, the forward chemical reaction rate constant k_f is due only to the ECR process. Our data fit the ECE profile with a ratio of n_2 to n_1 of ∼6 (Figures 3b and S7). Since the potential step to −1.4 V only forms H_2 and CO through competing pathways and the HER is slower than CO (as shown from the Tafel analysis in Figure 1d,e), we can conclude that the first electrochemical step (n_1) corresponds to the first electron transfer to form CO_2^-, while the second electrochemical step (n_2) is likely due to a combination of electrons transferred from the HER and the second electrochemical step to form CO (see Section S4 for an extended discussion on understanding fitting parameters).

Insights from the Cottrell analysis have important implications for refining the reaction mechanism and point to the clear role of sequential charge transfer and chemical reaction sub-processes in the early stages of the ECR reaction sequence. In general, the presence of an ECE-type deviation from the Cottrell line allows us to refine the possible reaction pathways to those that include an interposed homogeneous chemical reaction while eliminating other candidate pathways that do not. In the specific question of delineating between the coupled and decoupled proton−electron transfer pathways (iia and iib in Figure 1a, respectively), we can point to the characteristic deviation from the Cottrell line as a clear sign to support the sequential pathway while eliminating the concerted pathway. We note that this interpretation is further corroborated by a recent study by Deng et al.,[41] who used pH and kinetic isotope effect studies to identify the decoupled CO_2 adsorption step in pathway (iib) as the only plausible rate-limiting step in CO formation on Au, Ag, Sn, and In (Table S1). Deng et al. found that the RDS reaction order for H^+ and H_2O should be zero, leaving CO_2 adsorption to form $*CO_2^-$ as the only possible RDS.[41] Our results and Deng's results also corroborate findings by Chernyshova et al., who obtained direct spectroscopic evidence of the $*CO_2^-$ intermediate.[54]

Having established the analytical workflow, the chronoamperometric analysis, and the inferences about the reaction mechanism associated with the signatures of sequential electrochemical and chemical reactions, we now focus on the ECR and HER in a step change to a more negative applied potential. (−1.6 V). Based on the Tafel analysis shown in Figure 1, we note that this step to higher overpotential results in an approximately 10-fold increase in current density compared to the step to −1.4 V discussed above. Aside from the higher overall rates, analyzing the reaction under these conditions is complicated by forming a broader distribution of products (see Figure 1b). Nevertheless, we will show below that chronoamperometric analysis affords valuable insights into the interplay of reaction pathways.

The HER remains diffusion-limited at a potential step to −1.6 V, as evident from the control experiment of an Ar-saturated electrolyte (black trace, Figure 4). To establish a robust control, we also carried out an Ar-saturated control experiment in a 1 M KCl + 0.0016 M HCl solution (pH = 3.8), observing that in the absence of CO_2, the transient HER current decays linearly with $t^{-1/2}$ (Section S12). As an additional control experiment, we performed a potential step experiment to −1.6 V in $KHCO_3$ to validate that in the case of a buffered electrolyte (i.e., a constant pH, although the surface pH is greater than the bulk pH[55]), the transient signature is still consistent with a decoupled electrochemical and chemical reaction sequence (Section S13) and not a result of changing pH. As expected, the different product distributions in KCl versus $KHCO_3$ result in different current responses, so the corresponding ECE equation fit parameters differ. However, based on the presence of a nonlinear Cottrell response in both KCl and $KHCO_3$ electrolytes, we can confidently conclude that pH transients during the chronoamperometric measurements do not impact the transient current response and mechanistic interpretation. We would expect varying Cottrell responses for differing catalytic systems due to the different

https://doi.org/10.1021/acscatal.2c06043
ACS Catal. 2023, 13, 4938−4948

products being made, and these various catalytic systems (different catalysts, single facets, different electrolytes, etc.) are of interest for future studies to examine the reaction mechanism for different ECR products.

In the case of a CO_2-saturated electrolyte, the transient current of the ECR again shows a characteristic response with three distinctive deviations from the Cottrell line. First, at short times, up to about 4 s after the potential step, the observed transient current is significantly below the current corresponding to the fit of the Cottrell line. This deviation is generally attributed to kinetic complications in the form of Ohmic drops, electrochemical irreversibility, or pre-kinetics.[50,56] Since the RC time constant of our experimental setup is less than 1 ms (Section S3),[57] we can eliminate Ohmic drops as the cause. Instead, we attribute the initial deviation to pre-kinetics, as described in Figure 2. Specifically, considering the sequence of reaction steps illustrated in Figure 1a on the path to C_2 formation and the ECE characteristics evident from Figure 3 to forming *CO, we conclude that the kinetic limitation at short times is due to the kinetics of the chemical step (i.e., hydrogenation) identified above in the analysis at −1.4 V.

The second notable deviation from the Cottrell line is a dip in the transient current near $\sqrt{1/t} \sim 0.25\ s^{-1/2}$ ($t \gtrsim 5$ s). This dip could arise from a mass transfer limitation of an intermediate involved in the chemical reaction step or a nucleation-type phenomenon (e.g., bubble formation for gaseous products). The mass transfer limitations could involve several species, including the transport of hydrated protons to the catalyst surface or the nucleation of bubbles of gaseous products away from the catalyst surface. Rigorous rotating disk studies could, in principle, provide more insights into the mass transport conditions at the surface to confirm this hypothesis; however, this would be inconsistent with the underlying assumptions of the Cottrell analysis and is not the focus of our current work.

The third characteristic deviation is a shift toward a much steeper slope at long times due to the second Cottrell slope being proportional to the number of electrons in both electrochemical steps. Based on the same fitting algorithm applied above, we determine the n_2 to n_1 ratio to be about 10 (Figure S7). The n_2/n_1 ratio for the step to −1.6 V is larger than the n_2/n_1 of ∼ 6 observed for the step to −1.4 V discussed earlier. We attribute this trend to the increasing number of reactions taking place as we are making CO, CH_4, C_2H_4, HCOOH, and H_2.

The chronoamperometric analysis allows us to draw several strong inferences about the reaction mechanism, in particular with regard to reaction pathways to form C_2H_4, which is the major ECR product formed at −1.6 V. *CO is an essential and necessary intermediate in the formation of C_2H_4.[39,44] However, it has also been shown that CO and CO_2 require the same overpotential to produce hydrocarbons, which suggests that the rate-determining step occurs after the formation of an adsorbed CO intermediate.[6] The C−C coupling process is known to define a key step in the C_2 reaction pathway, with studies pointing to *CHO, *OCCO, and $*C_2O_2^-$ formation as the rate-determining intermediates.[40,43,47,58−63] Combining the established mechanistic understanding with new insights into the ECE mechanism evident from the analysis in Figure 4 leads us to conclude that the C_2 formation pathway cannot be explained by a concerted proton and electron transfer step. Instead, the ECE signatures from our analysis suggest that the C_2 formation pathway at −1.6 V vs Ag/AgCl involves a homogeneous chemical reaction interposed between two electrochemical steps. To present this interpretation in the context of a reaction pathway diagram, we examine the possible mechanism pathways summarized by Nitopi et al. (Figure 5).[14] We note that C−C coupling

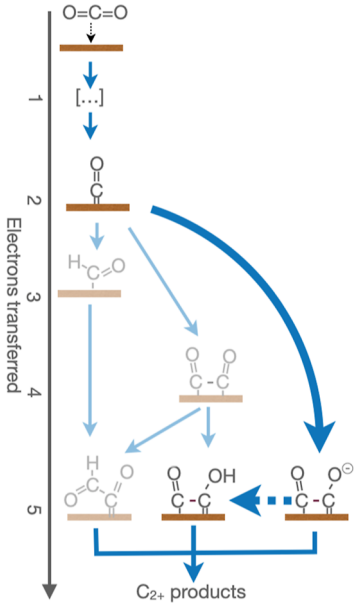

Figure 5. Simplified reaction pathway adopted from Nitopi et al.[14] to focus on proposed rate-limiting species from *CO through *CHO, *OCCO, and $*OCCO^-$ intermediates to C_2 products. The solid arrow indicates the electron transfer step (E), whether ET or PCET, and the dashed arrow indicates a separate chemical step (C) with no ET. Bold arrows indicate the most likely pathway based on our ECE analysis.

pathways have been previously shown to be potential dependent, with the coupling between *CO and *CO being preferred at lower overpotentials and the coupling between *CO and *CHO being preferred at higher overpotentials.[64,65] Among the candidate pathways illustrated in Figure 5, we can identify *CO → $*OCCO^-$ → *OCCOH → onward as the most likely pathway at −1.6 V vs Ag/AgCl in 1 M KCl. Via the process of elimination, we can rule out the other candidate pathways that do not include a separate chemical step evident from the ECE analysis of our experiments. Notably, this inference is corroborated by previous experimental and theoretical studies that support our finding that C_2H_4 formation proceeds via $*C_2O_2^-$ through separate electron−proton transfer steps. DFT calculations identified that the formation of the negatively charged CO dimer is most stable on Cu(100),[66] which is the predominantly exposed facet on our copper foil (Section S6). Theory, experiments, and DFT calculations identified that decoupled electron and proton transfer steps are the most likely pathway to C_2H_4 formation and that proton transfer happens only after the formation of the $*C_2O_2^-$ anionic dimer.[47,58,61,67] Ethylene formation has been found to be pH independent,[63,68,69] and a recent review by Varela summarizes that pH independent paths toward CO and C_2H_4 formation proceed through $*CO_2^-$ and $*C_2O_2^-$ intermediates, respectively,[70] further corroborating our mechanistic pathway findings.

https://doi.org/10.1021/acscatal.2c06043
ACS Catal. 2023, 13, 4938−4948

CONCLUSIONS

In summary, we show that the chronoamperometric analysis of the ECR reaction provides important mechanistic insights into reaction pathways and rate-limiting steps. Analysis of characteristic deviations from the Cottrell line allowed us to disentangle the interplay of mass transport and the sequence of electrochemical and chemical reactions. Specifically, our analysis provides two critical new insights. First, we show that the initial steps in ECR in an unbuffered KCl solution at −1.4 V to form CO involve sequential charge transfer and homogeneous chemical reactions (hydrogenation of $*CO_2$). Second, ECR at slightly higher overpotentials (−1.6 V) in an unbuffered KCl solution to form C_2H_4 involves a similar sequential pathway of the homogeneous chemical reaction interposed between electrochemical, which allows us to refine the possible reaction pathways to form C_2 products. The relatively simple yet underappreciated, chronoamperometric analysis, therefore, provides a powerful diagnostic tool to resolve outstanding mechanistic questions in ECR and other multi-step electrochemical reaction pathways. We hope that these results inspire more researchers to adopt chronoamperometric analysis in their experimental characterization and that the emerging mechanistic insights can translate toward more efficient and selective ECR systems to valorize CO_2 as a chemical feedstock.

METHODS

Electrode Fabrication and Electrolyte Preparation. The working electrode was a polycrystalline copper foil (puratronic, 99.9999%) connected to titanium wire (Aldrich) with silver paint (Leitsilber 200, Ted Pella Inc.). The back and edges were then covered with an inert epoxy (Omegabond 101), leaving an exposed geometric surface area of ∼0.2 cm^2. Prior to using in the cell, the electrode was electropolished in 85% phosphoric acid (Macron Fine Chemicals) to remove any impurities and surface oxides, leaving a mirror finish. After electropolishing, the electrode was thoroughly rinsed with DI water and immediately put into the cell.

The 1 M electrolyte was prepared with KCl (Sigma-Aldrich, ACS Reagent 99.0−100.5%) and 18.2 MΩ DI water (ELGA LabWater) and then stirred with chelex resin (Chelex100, sodium form, Sigma-Aldrich) for at least 24 h prior to usage.[71,72] CO_2-saturated KCl has a pH of ∼3.8.[57]

Electrochemical Measurements and Product Characterization. All experiments were performed at room temperature. The cell used was a custom-made two-compartment glass H-cell with a Cu foil working electrode, a Ag/AgCl reference electrode (Pine Instruments), a platinum mesh counter electrode (99.9999%, Alfa Aesar), and a Nafion 117 cation exchange membrane separating the anode and cathode compartments. Potentials were applied and 85% *iR* compensated in situ using a Biologic SP-300 potentiostat. The remaining 15% uncompensated *iR* drop is insignificant and is reported in Section S9. All experiments were performed at room temperature. The electrolyte was saturated with CO_2 (Research 5.0 grade, Airgas) for at least 30 min prior to applying a potential, and during the experiments, CO_2 was bubbled through at a controlled rate of 1.4 sccm using a mass flow controller (Bronkhorst EL-FLOW Select series). We recognize that this could disrupt the electrode surface; however, it is a small perturbation far from the electrode and does not negate the use of the Cottrell equation (Section S8). The cell outlet was connected directly to a gas chromatograph (SRI, Multigas no. 5) equipped with FID and TCD detectors. Argon (Airgas) was used as a carrier gas, and hydrogen from a hydrogen generator (H2-100, SRI Instruments) was used for the FID. Liquid aliquots were taken at the end for ^1H NMR analysis (Bruker AV-500). The NMR samples were prepared by mixing an aliquot of the electrolyte after measurement with D_2O (99.9 atom % D, Aldrich) and a 500 μM dimethyl sulfoxide (Fisher Chemical) solution in a 1:1:8 volume ratio.

Product characterization took place 10 min into electrolysis. Each run takes 18 min with an 8 min cooldown period, so we collect one set of data every 26 min. The coulombs needed to produce that concentration of each product were calculated and divided by the total coulombs needed to make all measured products to determine the current efficiency. The partial current density for a given product was calculated by multiplying the total current density by the corresponding product's current efficiency.

Chronoamperometry/sampled voltammetry data were collected by holding the potential at −0.6 V for 2 min and then stepping to the specified cathodic potential, recording current values every 100 ms. The potential of −0.6 V vs Ag/AgCl (equivalent to ∼ −0.18 V_{RHE}) was selected to ensure complete reduction of any residual oxides before measurements. Work by Wahab et al. found that stripping of the passive layer formed on polycrystalline copper in air has an onset potential of about −0.16 V_{RHE} on the Cu(100) facet,[73] which is the predominant exposed facet on our polycrystalline copper foil.[74] I vs $t^{-1/2}$ data were plotted for t = 200 ms and on to minimize the double layer charging current contributions. From previous work in KCl and from calculations in Section S3, the RC time constant was found to be on the order of a few milliseconds or less.[57] At the end of the experiments, the electrode still had a mirror finish, indicating minimal roughening, which was supported by our roughness factor measurements. Though the electrode experienced minimal roughening, it is possible that the formation of gas bubbles, which block active surface sites and decrease the electrochemically active surface area, caused uncertainty in the geometric surface area, which we used to calculate current density. This effect would become significant at high overpotentials and the resulting high current densities, leading to noisy chronoamperometry data, which could make mechanistic interpretation more difficult.

Linear sweep voltammograms (LSVs) were collected from −0.3 V vs Ag/AgCl to −2 V at a scan rate of 10 mV/s in CO_2-saturated electrolyte. The roughness factor was approximated by comparing the post-experiment double layer capacitance to the initial double layer capacitance. Double layer capacitance was estimated by collecting cyclic voltammetry scans from −0.27 to −0.42 V vs Ag/AgCl at increasing scan rates. In this potential window, there are no Faradaic processes. The width of the scan at −0.32 V was then plotted versus scan rate, where the slope is equivalent to the double layer capacitance.

ECE Fit. Chronoamperometry data were fit to the ECE equation (eq 4) using a nonlinear least squares method in Python called scipy.optimize.curve_fit. The parameters n_1, n_2, k_f, and a were confined between 0 and ∞. The curve fit method finds the optimal set of parameters for the defined function that best fits the provided data set. The specific least squares method used in the curve fit function was the default trust region reflective algorithm.

https://doi.org/10.1021/acscatal.2c06043
ACS Catal. 2023, 13, 4938−4948

■ ASSOCIATED CONTENT

Supporting Information

The Supporting Information is available free of charge at https://pubs.acs.org/doi/10.1021/acscatal.2c06043.

Comparison of LSV and potentiostatic measurements, Tafel plot analysis, electrode surface roughening analysis from double layer capacitance, detailed description of the Cottrell fitting algorithm, possible reaction pathways from CO_2 to CO, analysis of the electrode structure, validation of the assumption of isothermal conditions, pH and electrolyte control experiments, and gas chromatography and NMR analysis (PDF)

■ AUTHOR INFORMATION

Corresponding Author

Tobias Hanrath − *Robert F. Smith School of Chemical and Biomolecular Engineering, Cornell University, Ithaca, New York 14853, United States;* orcid.org/0000-0001-5782-4666; Email: th358@cornell.edu

Authors

Rileigh Casebolt DiDomenico − *Robert F. Smith School of Chemical and Biomolecular Engineering, Cornell University, Ithaca, New York 14853, United States;* orcid.org/0000-0002-1134-1666

Kelsey Levine − *Robert F. Smith School of Chemical and Biomolecular Engineering, Cornell University, Ithaca, New York 14853, United States*

Laila Reimanis − *Applied and Engineering Physics, Cornell University, Ithaca, New York 14853, United States;* orcid.org/0000-0002-9341-5015

Héctor D. Abruña − *Chemistry and Chemical Biology, Ithaca, New York 14853, United States;* orcid.org/0000-0002-3948-356X

Complete contact information is available at: https://pubs.acs.org/10.1021/acscatal.2c06043

Notes

The authors declare no competing financial interest.

■ ACKNOWLEDGMENTS

This work was supported in part by the National Science Foundation (NSF) CBET1805400. R.C.D. was supported by the CESI-Corning Graduate Fellowship. K.L. and L.R. acknowledge support from the Cornell Engineering Learning Initiative. This work made use of the Cornell University NMR Facility, which is supported, in part, by the NSF through MRI award CHE-1531632. We thank Michael DiDomenico for his assistance with curve fitting parameter estimation.

■ REFERENCES

(1) Yu, J.; Wang, J.; Ma, Y.; Zhou, J.; Wang, Y.; Lu, P.; Yin, J.; Ye, R.; Zhu, Z.; Fan, Z. Recent progresses in electrochemical carbon dioxide reduction on copper-based catalysts toward multicarbon products. *Adv. Funct. Mater.* **2021**, *31*, 2102151.

(2) Li, M.; Wang, H.; Luo, W.; Sherrell, P. C.; Chen, J.; Yang, J. Heterogeneous single-atom catalysts for electrochemical CO2 reduction reaction. *Adv. Mater.* **2020**, *32*, 2001848.

(3) Lu, Q.; Jiao, F. Electrochemical CO2 reduction: Electrocatalyst, reaction mechanism, and process engineering. *Nano Energy* **2016**, *29*, 439−456.

(4) Zheng, Y.; Vasileff, A.; Zhou, X.; Jiao, Y.; Jaroniec, M.; Qiao, S.-Z. Understanding the roadmap for electrochemical reduction of CO2 to multi-carbon oxygenates and hydrocarbons on copper-based catalysts. *J. Am. Chem. Soc.* **2019**, *141*, 7646−7659.

(5) Kumar, B.; Brian, J. P.; Atla, V.; Kumari, S.; Bertram, K. A.; White, R. T.; Spurgeon, J. M. New trends in the development of heterogeneous catalysts for electrochemical CO_2 reduction. *Catal. Today* **2016**, *270*, 19−30.

(6) Fan, L.; Xia, C.; Yang, F.; Wang, J.; Wang, H.; Lu, Y. Strategies in catalysts and electrolyzer design for electrochemical CO_2 reduction toward C2+ products. *Sci. Adv.* **2020**, *6*, No. eaay3111.

(7) Xiao, C.; Zhang, J. Architectural design for enhanced C2 product selectivity in electrochemical CO_2 reduction using Cu-based catalysts: a review. *ACS Nano* **2021**, *15*, 7975−8000.

(8) Ni, Z.; Liang, H.; Yi, Z.; Guo, R.; Liu, C.; Liu, Y.; Sun, H.; Liu, X. Research progress of electrochemical CO_2 reduction for copper-based catalysts to multicarbon products. *Coord. Chem. Rev.* **2021**, *441*, 213983.

(9) Rabiee, H.; Ge, L.; Zhang, X.; Hu, S.; Li, M.; Yuan, Z. Gas diffusion electrodes (GDEs) for electrochemical reduction of carbon dioxide, carbon monoxide, and dinitrogen to value-added products: a review. *Energy Environ. Sci.* **2021**, *14*, 1959−2008.

(10) Wakerley, D.; Lamaison, S.; Wicks, J.; Clemens, A.; Feaster, J.; Corral, D.; Jaffer, S. A.; Sarkar, A.; Fontecave, M.; Duoss, E. B.; Baker, S.; Sargent, E. H.; Jaramillo, T. F.; Hahn, C. Gas diffusion electrodes, reactor designs and key metrics of low-temperature CO_2 electrolysers. *Nat. Energy* **2022**, *7*, 130−143.

(11) Yang, Y.; Li, F. Reactor design for electrochemical CO_2 conversion toward large-scale applications. *Curr. Opin. Green Sustainable Chem.* **2021**, *27*, 100419.

(12) Ma, D.; Jin, T.; Xie, K.; Huang, H. An overview of flow cell architectures design and optimization for electrochemical CO_2 reduction. *J. Mater. Chem. A* **2021**, *9*, 20897.

(13) Kuhl, K. P.; Cave, E. R.; Abram, D. N.; Jaramillo, T. F. New insights into the electrochemical reduction of carbon dioxide on metallic copper surfaces. *Energy Environ. Sci.* **2012**, *5*, 7050−7059.

(14) Nitopi, S.; Bertheussen, E.; Scott, S. B.; Liu, X.; Engstfeld, A. K.; Horch, S.; Seger, B.; Stephens, I. E.; Chan, K.; Hahn, C.; Nørskov, J. K.; Jaramillo, T. F.; Chorkendorff, I. Progress and perspectives of electrochemical CO_2 reduction on copper in aqueous electrolyte. *Chem. Rev.* **2019**, *119*, 7610−7672.

(15) Bagger, A.; Ju, W.; Varela, A. S.; Strasser, P.; Rossmeisl, J. Electrochemical CO_2 reduction: a classification problem. *ChemPhysChem* **2017**, *18*, 3266−3273.

(16) Kibria, M. G.; Edwards, J. P.; Gabardo, C. M.; Dinh, C. T.; Seifitokaldani, A.; Sinton, D.; Sargent, E. H. Electrochemical CO_2 reduction into chemical feedstocks: from mechanistic electrocatalysis models to system design. *Adv. Mater.* **2019**, *31*, 1807166.

(17) Resasco, J.; Chen, L. D.; Clark, E.; Tsai, C.; Hahn, C.; Jaramillo, T. F.; Chan, K.; Bell, A. T. Promoter effects of alkali metal cations on the electrochemical reduction of carbon dioxide. *J. Am. Chem. Soc.* **2017**, *139*, 11277−11287.

(18) Kim, C.; Bui, J. C.; Luo, X.; Cooper, J. K.; Kusoglu, A.; Weber, A. Z.; Bell, A. T. Tailored catalyst microenvironments for CO_2 electroreduction to multicarbon products on copper using bilayer ionomer coatings. *Nat. Energy* **2021**, *6*, 1026−1034.

(19) Varela, A. S.; Kroschel, M.; Reier, T.; Strasser, P. Controlling the selectivity of CO_2 electroreduction on copper: The effect of the electrolyte concentration and the importance of the local pH. *Catal. Today* **2016**, *260*, 8−13.

(20) Gao, D.; Sinev, I.; Scholten, F.; Arán-Ais, R. M.; Divins, N. J.; Kvashnina, K.; Timoshenko, J.; Roldan Cuenya, B. Selective CO_2 electroreduction to ethylene and multicarbon alcohols via electrolyte-driven nanostructuring. *Angew. Chem.* **2019**, *131*, 17203−17209.

(21) Fu, Y.; Xie, Q.; Wu, L.; Luo, J. Crystal facet effect induced by different pretreatment of Cu2O nanowire electrode for enhanced electrochemical CO_2 reduction to C2+ products. *Chin. J. Catal.* **2022**, *43*, 1066−1073.

(22) Jiang, K.; Sandberg, R. B.; Akey, A. J.; Liu, X.; Bell, D. C.; Nørskov, J. K.; Chan, K.; Wang, H. Metal ion cycling of Cu foil for

selective C−C coupling in electrochemical CO_2 reduction. *Nat. Catal.* **2018**, *1*, 111−119.
(23) Li, C. W.; Kanan, M. W. CO_2 reduction at low overpotential on Cu electrodes resulting from the reduction of thick Cu2O films. *J. Am. Chem. Soc.* **2012**, *134*, 7231−7234.
(24) Jiang, K.; Huang, Y.; Zeng, G.; Toma, F. M.; Goddard, W. A., III; Bell, A. T. Effects of surface roughness on the electrochemical reduction of CO_2 over Cu. *ACS Energy Lett.* **2020**, *5*, 1206−1214.
(25) Mistry, H.; Varela, A. S.; Bonifacio, C. S.; Zegkinoglou, I.; Sinev, I.; Choi, Y.-W.; Kisslinger, K.; Stach, E. A.; Yang, J. C.; Strasser, P.; Cuenya, B. R. Highly selective plasma-activated copper catalysts for carbon dioxide reduction to ethylene. *Nat. Commun.* **2016**, *7*, 1−9.
(26) Lee, S. Y.; Jung, H.; Kim, N.-K.; Oh, H.-S.; Min, B. K.; Hwang, Y. J. Mixed copper states in anodized Cu electrocatalyst for stable and selective ethylene production from CO_2 reduction. *J. Am. Chem. Soc.* **2018**, *140*, 8681−8689.
(27) Wang, J.; Tan, H. Y.; Zhu, Y.; Chu, H.; Chen, H. M. Linking the dynamic chemical state of catalysts with the product profile of electrocatalytic CO_2 reduction. *Angew. Chem.* **2021**, *133*, 17394−17407.
(28) Yuan, X.; Chen, S.; Cheng, D.; Li, L.; Zhu, W.; Zhong, D.; Zhao, Z. J.; Li, J.; Wang, T.; Gong, J. Controllable Cu 0 -Cu + Sites for Electrocatalytic Reduction of Carbon Dioxide. *Angew. Chem.* **2021**, *133*, 15472−15475.
(29) Ruiz-López, E.; Gandara-Loe, J.; Baena-Moreno, F.; Reina, T. R.; Odriozola, J. A. Electrocatalytic CO_2 conversion to C2 products: Catalysts design, market perspectives and techno-economic aspects. *Renewable Sustainable Energy Rev.* **2022**, *161*, 112329.
(30) Cao, G.; Cao, X.; Shan, M.; Li, M.; Zhu, X.; Han, J.; Ge, Q.; Wang, H. Surface cavity effect on C2H4 formation from electrochemical reduction of CO_2 as studied using Cu2O cubes. *J. Solid State Electrochem.* **2022**, *26*, 1527−1540.
(31) Gustavsen, K. R.; Wang, K. Recent advances on enhancing the multicarbon selectivity of nanostructured Cu-based catalysts. *Phys. Chem. Chem. Phys.* **2021**, *23*, 12514−12532.
(32) Kim, C.; Weng, L.-C.; Bell, A. T. Impact of pulsed electrochemical reduction of CO_2 on the formation of C2+ products over Cu. *ACS Catal.* **2020**, *10*, 12403−12413.
(33) Arán-Ais, R. M.; Scholten, F.; Kunze, S.; Rizo, R.; Roldan Cuenya, B. The role of in situ generated morphological motifs and Cu(I) species in C2+ product selectivity during CO_2 pulsed electroreduction. *Nat. Energy* **2020**, *5*, 317−325.
(34) Timoshenko, J.; Bergmann, A.; Rettenmaier, C.; Herzog, A.; Arán-Ais, R. M.; Jeon, H. S.; Haase, F. T.; Hejral, U.; Grosse, P.; Kühl, S.; Davis, E. M.; Tian, J.; Magnussen, O.; Roldan Cuenya, B. Steering the structure and selectivity of CO_2 electroreduction catalysts by potential pulses. *Nat. Catal.* **2022**, *5*, 259−267.
(35) DiDomenico, R. C.; Hanrath, T. Pulse Symmetry Impacts the C2 Product Selectivity in Pulsed Electrochemical CO_2 Reduction. *ACS Energy Lett.* **2021**, *7*, 292−299.
(36) Tang, Z.; Nishiwaki, E.; Fritz, K. E.; Hanrath, T.; Suntivich, J. Cu(I) reducibility controls ethylene vs ethanol selectivity on (100)-textured copper during pulsed CO_2 reduction. *ACS Appl. Mater. Interfaces* **2021**, *13*, 14050−14055.
(37) Resasco, J.; Abild-Pedersen, F.; Hahn, C.; Bao, Z.; Koper, M.; Jaramillo, T. F. Enhancing the connection between computation and experiments in electrocatalysis. *Nat. Catal.* **2022**, *5*, 374−381.
(38) de Ruiter, J.; An, H.; Wu, L.; Gijsberg, Z.; Yang, S.; Hartman, T.; Weckhuysen, B. M.; van der Stam, W. Probing the Dynamics of Low-Overpotential CO_2-to-CO Activation on Copper Electrodes with Time-Resolved Raman Spectroscopy. *J. Am. Chem. Soc.* **2022**, *144*, 15047.
(39) An, H.; Wu, L.; Mandemaker, L. D.; Yang, S.; Ruiter, J.; Wijten, J. H.; Janssens, J. C.; Hartman, T.; Stam, W.; Weckhuysen, B. M. Sub-Second Time-Resolved Surface-Enhanced Raman Spectroscopy Reveals Dynamic CO Intermediates during Electrochemical CO_2 Reduction on Copper. *Angew. Chem., Int. Ed.* **2021**, *60*, 16576−16584.
(40) Kim, Y.; Park, S.; Shin, S.-J.; Choi, W.; Min, B. K.; Kim, H.; Kim, W.; Hwang, Y. J. Time-resolved observation of C−C coupling intermediates on Cu electrodes for selective electrochemical CO_2 reduction. *Energy Environ. Sci.* **2020**, *13*, 4301−4311.
(41) Deng, W.; Zhang, P.; Seger, B.; Gong, J. Unraveling the rate-limiting step of two-electron transfer electrochemical reduction of carbon dioxide. *Nat. Commun.* **2022**, *13*, 1−9.
(42) Peterson, A. A.; Abild-Pedersen, F.; Studt, F.; Rossmeisl, J.; Nørskov, J. K. How copper catalyzes the electroreduction of carbon dioxide into hydrocarbon fuels. *Energy Environ. Sci.* **2010**, *3*, 1311−1315.
(43) Clark, E.; Bell, A. Chapter 3: Heterogeneous Electrochemical CO_2 Reduction. In *Carbon Dioxide Electrochemistry: Homogeneous and Heterogeneous Catalysis*; Robert, M., Costentin, C., Daasbjerg, K., Eds.; Royal Society of Chemistry: London, 2021; pp 98−150.
(44) Zhan, C.; Dattila, F.; Rettenmaier, C.; Bergmann, A.; Kühl, S.; García-Muelas, R.; López, N. r.; Cuenya, B. R. Revealing the CO coverage-driven C−C coupling mechanism for electrochemical CO_2 reduction on Cu2O nanocubes via operando Raman spectroscopy. *ACS Catal.* **2021**, *11*, 7694−7701.
(45) Hori, Y.; Murata, A.; Takahashi, R. Formation of hydrocarbons in the electrochemical reduction of carbon dioxide at a copper electrode in aqueous solution. *J. Chem. Soc., Faraday Trans. 1* **1989**, *85*, 2309−2326.
(46) Grahame, D. C. The electrical double layer and the theory of electrocapillarity. *Chem. Rev.* **1947**, *41*, 441−501.
(47) Kortlever, R.; Shen, J.; Schouten, K. J. P.; Calle-Vallejo, F.; Koper, M. T. Catalysts and reaction pathways for the electrochemical reduction of carbon dioxide. *J. Phys. Chem. Lett.* **2015**, *6*, 4073−4082.
(48) Bard, A.; Faulkner, L. *Electrochemical Methods: Fundamentals and Applications*, 2nd ed.; John Wiley & Sons, Inc., 2001.
(49) Limaye, A. M.; Zeng, J. S.; Willard, A. P.; Manthiram, K. Bayesian data analysis reveals no preference for cardinal Tafel slopes in CO_2 reduction electrocatalysis. *Nat. Commun.* **2021**, *12*, 1−10.
(50) Murray, R. Chronoamperometry, Chronocoulometry, and Chronopotentiometry. In *Techniques of Chemistry*; Weissberger, A., Rossiter, B., Eds.; John Wiley & Sons, Inc., 1971; Vol. *I*, Part IIA, pp 591−644.
(51) Lee, S. H.; Sullivan, I.; Larson, D. M.; Liu, G.; Toma, F. M.; Xiang, C.; Drisdell, W. S. Correlating oxidation state and surface area to activity from operando studies of copper CO electroreduction catalysts in a gas-fed device. *ACS Catal.* **2020**, *10*, 8000−8011.
(52) Strain, J. M.; Gulati, S.; Pishgar, S.; Spurgeon, J. M. Pulsed Electrochemical Carbon Monoxide Reduction on Oxide-Derived Copper Catalyst. *ChemSusChem* **2020**, *13*, 3028−3033.
(53) Alberts, G. S.; Shain, I. Electrochemical Study of Kinetics of a Chemical Reaction Coupled between Two Charge Transfer Reactions. Potentiostatic Reduction of p-Nitrosophenol. *Anal. Chem.* **1963**, *35*, 1859−1866.
(54) Chernyshova, I. V.; Somasundaran, P.; Ponnurangam, S. On the origin of the elusive first intermediate of CO_2 electroreduction. *Proc. Natl. Acad. Sci. U.S.A.* **2018**, *115*, E9261−E9270.
(55) Gupta, N.; Gattrell, M.; MacDougall, B. Calculation for the cathode surface concentrations in the electrochemical reduction of CO_2 in KHCO3 solutions. *J. Appl. Electrochem.* **2006**, *36*, 161−172.
(56) Montella, C. Discussion of the potential step method for the determination of the diffusion coefficients of guest species in host materials: Part I. Influence of charge transfer kinetics and ohmic potential drop. *J. Electroanal. Chem.* **2002**, *518*, 61−83.
(57) Casebolt, R.; Kimura, K. W.; Levine, K.; Cimada DaSilva, J. A.; Kim, J.; Dunbar, T. A.; Suntivich, J.; Hanrath, T. Effect of electrolyte composition and concentration on pulsed potential electrochemical CO_2 reduction. *ChemElectroChem* **2021**, *8*, 681−688.
(58) Li, J.; Chang, X.; Zhang, H.; Malkani, A. S.; Cheng, M.-j.; Xu, B.; Lu, Q. Electrokinetic and in situ spectroscopic investigations of CO electrochemical reduction on copper. *Nat. Commun.* **2021**, *12*, 1−11.
(59) Liu, X.; Schlexer, P.; Xiao, J.; Ji, Y.; Wang, L.; Sandberg, R. B.; Tang, M.; Brown, K. S.; Peng, H.; Ringe, S.; Hahn, C.; Jaramillo, T. F.; Nørskov, J. K.; Chan, K. pH effects on the electrochemical

reduction of CO_2 towards C2 products on stepped copper. *Nat. Commun.* **2019**, *10*, 1−10.
(60) Ou, L.; He, Z.; Yang, H.; Chen, Y. Theoretical Insights into Potential-Dependent C−C Bond Formation Mechanisms during CO_2 Electroreduction into C2 Products on Cu (100) at Simulated Electrochemical Interfaces. *ACS Omega* **2021**, *6*, 17839−17847.
(61) Calle-Vallejo, F.; Koper, M. T. Theoretical considerations on the electroreduction of CO to C2 species on Cu (100) electrodes. *Angew. Chem., Int. Ed.* **2013**, *52*, 7282−7285.
(62) Montoya, J. H.; Peterson, A. A.; Nørskov, J. K. Insights into C-C Coupling in CO_2 Electroreduction on Copper Electrodes. *ChemCatChem* **2013**, *5*, 737−742.
(63) Hori, Y.; Takahashi, R.; Yoshinami, Y.; Murata, A. Electrochemical reduction of CO at a copper electrode. *J. Phys. Chem. B* **1997**, *101*, 7075−7081.
(64) Goodpaster, J. D.; Bell, A. T.; Head-Gordon, M. Identification of possible pathways for C−C bond formation during electrochemical reduction of CO_2: new theoretical insights from an improved electrochemical model. *J. Phys. Chem. Lett.* **2016**, *7*, 1471−1477.
(65) Liu, H.; Yang, B. Potential-dependent C-C coupling mechanism and activity of C2 formation in the electrocatalytic reduction of CO_2 on defective Cu(100) surfaces. *Chem. Commun.* **2022**, *58*, 709−712.
(66) Li, H.; Li, Y.; Koper, M. T.; Calle-Vallejo, F. Bond-making and breaking between carbon, nitrogen, and oxygen in electrocatalysis. *J. Am. Chem. Soc.* **2014**, *136*, 15694−15701.
(67) Koper, M. T. Theory of multiple proton−electron transfer reactions and its implications for electrocatalysis. *Chem. Sci.* **2013**, *4*, 2710−2723.
(68) Schouten, K. J. P.; Pérez Gallent, E. P.; Koper, M. T. The influence of pH on the reduction of CO and CO_2 to hydrocarbons on copper electrodes. *J. Electroanal. Chem.* **2014**, *716*, 53−57.
(69) Wang, L.; Nitopi, S. A.; Bertheussen, E.; Orazov, M.; Morales-Guio, C. G.; Liu, X.; Higgins, D. C.; Chan, K.; Nørskov, J. K.; Hahn, C.; Jaramillo, T. F. Electrochemical carbon monoxide reduction on polycrystalline copper: Effects of potential, pressure, and pH on selectivity toward multicarbon and oxygenated products. *ACS Catal.* **2018**, *8*, 7445−7454.
(70) Varela, A. S. The importance of pH in controlling the selectivity of the electrochemical CO_2 reduction. *Curr. Opin. Green Sustainable Chem.* **2020**, *26*, 100371.
(71) Jovanov, Z. P.; Ferreira de Araujo, J.; Li, S.; Strasser, P. Catalyst preoxidation and EDTA electrolyte additive remedy activity and selectivity declines during electrochemical CO_2 reduction. *J. Phys. Chem. C* **2019**, *123*, 2165−2174.
(72) Wuttig, A.; Surendranath, Y. Impurity ion complexation enhances carbon dioxide reduction catalysis. *ACS Catal.* **2015**, *5*, 4479−4484.
(73) Wahab, O. J.; Kang, M.; Daviddi, E.; Walker, M.; Unwin, P. R. Screening Surface Structure−Electrochemical Activity Relationships of Copper Electrodes under CO_2 Electroreduction Conditions. *ACS Catal.* **2022**, *12*, 6578−6588.
(74) Kimura, K. W.; Fritz, K. E.; Kim, J.; Suntivich, J.; Abruña, H. D.; Hanrath, T. Controlled selectivity of CO_2 reduction on copper by pulsing the electrochemical potential. *ChemSusChem* **2018**, *11*, 1781−1786.

https://doi.org/10.1021/acscatal.2c06043
ACS Catal. 2023, 13, 4938−4948